Eur. Phys. J. AP **3**, 287–293 (1998)

THE EUROPEAN PHYSICAL JOURNAL APPLIED PHYSICS

Heat transfer around a spherical particle levitated in argon plasma jet

P. Snabre[a], M. Announ, J.M. Badie, and B. Granier

Institut de Science et de Génie des Matériaux et Procédés[b], B.P.5, 66125 Font-Romeu, France

Received: 6 February 1998 /Revised: 25 June 1998 / Accepted: 28 June 1998

Abstract. This paper concerns momentum and heat transfer to a nonevaporating oxidized steel spherical particle (diameter 6.5 mm−8 mm) levitated at high Reynolds number in argon turbulent plasma jet flowing into cold air. The rapid rotation of the particle in the plasma flow ensures the stability of the levitation phenomenon over a wide range of plasma torch parameters. We use a dimensional analysis to describe the momentum transfer and the equilibrium levitation height data. The convective heat transfer coefficient was further estimated from gas and particle equilibrium temperature at the front stagnation point or from the analysis of the transient temperature signal for a particle abruptly immersed and levitated in the plasma jet. Particle rotation is shown to determine the heat transfer rate in a nonuniform plasma flow.

PACS. 47.27.-i Turbulent flows, convection, and heat transfer – 52.40.Hf Plasma-wall interactions; boundary layer effects; plasma sheats – 52.75.Hn Plasma torches

1 Introduction

Studies of heat and mass transfer to a solid body in a thermal plasma flow have been pursued during the past few decades because of the wide range of applications (plasma spraying, vitrification, plasma waste destruction) [1]. The few available experimental data are questionable since the particle is either injected across a nonuniform plasma arc [2] or supported in the flow by a tungsten wire [3]. Despite the steep temperature and velocity gradients experienced by the particle, the heat transfer is usually described by the well known Ranz Marshall relation [4] for an infinite flow and Reynolds number $10 < Re < 2000$:

$$Nu = 2 + 0.6Re^{1/2}Pr^{1/3} \quad (1)$$

where Nu is the Nusselt number and Pr the Prandtl number. Many experimental studies suggest correction factors that account for temperature gradient within the boundary layer around the particle, the Knudsen effect or the evaporation effect [5,6]. However, the transport correlations ignore both the plasma flow conditions and the particle rotation in nonuniform flows which could explain the significant deviation in the predicted heat flux based on correction factors. The problem of heat transfer from a particle rotating in a plasma flow has received little attention and theoretical studies mainly concern a uniform infinite flow [7,8].

This work concerns an original levitation technique to study equilibrium or transient heat transfer between a nonevaporating oxidized stainless steel sphere (surface temperature lower than the steel melting point ≈ 1750 K) and a turbulent plasma jet. The levitation method eliminates artifacts arising from a supporting wire and makes possible investigation of the effects of free particle rotation on heat transfer in a nonuniform plasma flow.

2 Levitation experiments, plasma characterization

The thermal plasma flow is produced by a d.c. plasma jet generator (arc currents 60 A $< I <$ 300 A with ±1% accuracy and arc voltages 20 V with ±2% accuracy). The argon plasma is generated by the arc current between the tungsten cathode and the copper anode nozzle (inner diameter of the exit section of the nozzle 2.5 mm $\leq D \leq$ 4 mm) both protected from thermal damage by water cooling. The argon flows upward as a plasma jet from the generator nozzle into the room temperature air. A stainless steel spherical particle of diameter d (6.5 mm $\leq d \leq$ 8 mm) is aerodynamically levitated in the argon plasma jet with gas flow rates 5×10^{-3} m^3/mn $\leq Q \leq 1.1 \times 10^{-2}$ m^3/mn.

The shifted radial position of the solid sphere away from the jet axis (Figs. 1b and 1c) induces a rotation couple. The horizontal inertial force $\mathbf{F}_\omega^\perp$ (Magnus force resulting from particle rotation) perpendicular to the flow direction then contributes to the stability of the levitation mechanism (Fig. 2).

Under high torch power conditions (energy supplied to the plasma $P >$ 1.9 kW), the particle surface temperature exceeds the steel melting point ($T_p \approx$ 1750 K)

[a] e-mail: snabre@imp-odeillo.fr
[b] UPR 8521

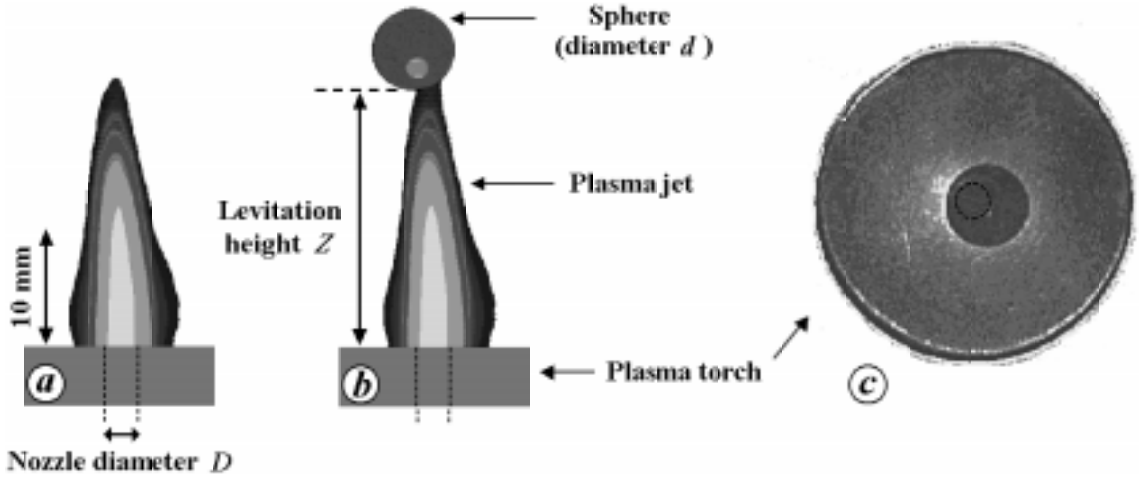

Fig. 1. Visualization imagery of the plasma flow (a) and the spherical steel particle levitated in argon plasma jet ((b) front view, (c) top view).

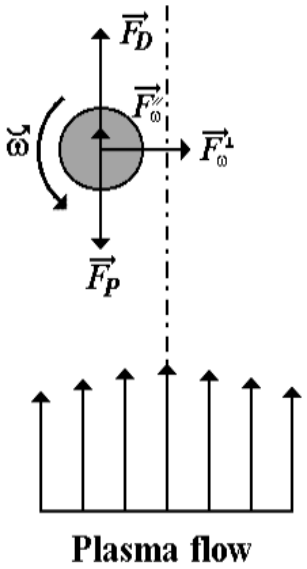

Fig. 2. Schematic drawing of forces acting on a particle levitated in a thermal plasma jet.

and then liquid droplets are expelled from the rotating particle (Fig. 3a). The linear velocity $u(r)$ of expelled droplets yields an estimate of the particle rotation speed $\omega \approx 2u(d)/d$. The visualization of liquid droplets motion with a CCD camera equipped with an electronic shutter gives a rotation speed increasing with the net torch power and ranging from 900 s^{-1} to 1500 s^{-1} for $P = 1.9$ kW (Fig. 3b).

We may thus neglect the inertial force $\mathbf{F}_\omega^{\parallel}$ in the flow direction (Fig. 2) since the gas velocity $U \approx 100$ m/s $-$ -300 m/s is larger than the tangential velocity $d\omega/2$ of the rotating sphere [9].

$$\left|\mathbf{F}_\omega^{\parallel}\right| \approx \rho S \omega^2 d^2 \approx \left|\mathbf{F}_\omega^{\perp}\right| \left(\frac{\omega d}{U}\right)^2$$
$$\text{with} \quad \mathbf{F}_\omega^{\perp} \approx \rho S \mathbf{U} \wedge \boldsymbol{\omega} \qquad (2)$$

where ρ is the plasma density and S the sphere area. Therefore, the force balance between the drag force $\mathbf{F}_D$ and the particle weight $\mathbf{F}_P$ ($F_D = F_P = mg$ where m is the particle mass and g the gravitational acceleration) determines the levitation height Z (vertical distance from the front stagnation point to the nozzle exit plane, Fig. 1b). Experiments with a drag probe and a supporting tungsten wire in the wake of the sphere located at the equilibrium levitation height in the argon plasma jet indeed gives $F_D(\omega = 0, Z)/mg \approx 1.05 - 1.15$ where $F_D(\omega = 0, Z)$ is the net drag experienced by a motionless particle [10]. This result agrees well with the force balance $F_D(\omega, Z) = mg$ and shows the weak influence of particle rotation since the additional contribution of the supporting wire leads to a slight increase $\approx 10\%$ of the net drag force [3].

A CCD video camera is used to visualize the sphere position in the plasma jet and to determine the levitation height Z (Fig. 1). The turbulent nature of the flow results in an experimental accuracy of about $\pm 5\%$ for the equilibrium levitation height Z. During the course of experiments, we can change the operating conditions (argon flow rate Q with $\pm 3\%$ accuracy and the net torch power P supplied to the plasma jet with $\pm 10\%$ accuracy) and the equilibrium levitation height Z.

The study of momentum and heat transfer requires information about gas temperatures and velocities in the thermal plasma. Considering the argon plasma as an ideal gas, the mean temperature T_O and gas velocity U_O near the jet exit (subscript "o") are derived with $\pm 15\%$ accuracy from the enthalpy balance:

$$P = \mathcal{Q}\rho_o C_{po}\left(T_o - T_a\right) + \frac{1}{2}\mathcal{Q}\rho_o\left(U_o^2 - U_a^2\right) \qquad (3)$$

where P is the power supplied to the plasma jet (net torch power), $\mathcal{Q} = \pi U_o D^2/4$ the volumetric flow rate, $C_{po} = 20.1$ $JM^{-1}K^{-1}$ the argon heat capacity, T_a the ambient air temperature (300 K) and $U_a = U_o T_a/T_o$ the argon velocity at the nozzle exit under laboratory pressure and temperature conditions.

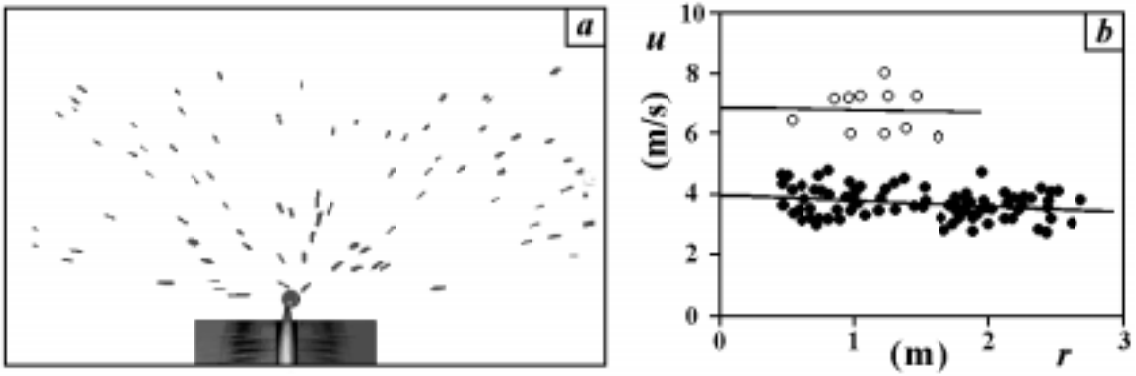

Fig. 3. Visualization imagery of liquid droplets expelled from the rotating particle in the argon plasma jet (a). Velocity $u(r)$ of liquid droplets *versus* the radial distance r from the particle (b) ((○) $d = 6$ mm, $P = 2700$ W, (●) $d = 6.5$ mm, $P = 1980$ W). Nozzle diameter $D = 3$ mm.

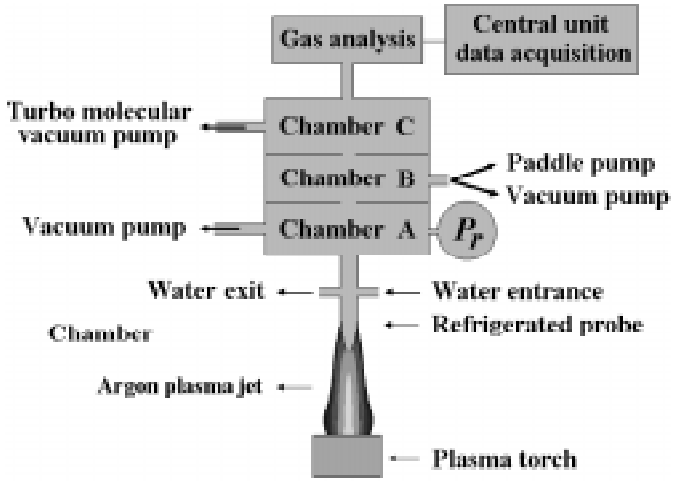

Fig. 4. Sample probe for the measurement of gas temperature and gas composition by mass spectrometry.

We have determined the plasma temperature in the turbulent mixing region by sampling gas with a water cooled probe near the argon jet axis and measuring the mass flow rate under low pressure p_r in a cold pipe (Fig. 4). However, the mass flow rate balance between hot and cold temperature conditions involves the plasma - air composition through the molar mass, the dynamic viscosity and the heat capacity of the gas species. We have then sampled gas in an additional low pressure chamber ($< 10^{-6}$ Torr) connected to a mass spectrometer. The gas sample at this orifice is sufficiently small so as to have no significant influence on the mass flow rate balance. From mass spectrometry data about the cold gas composition and a thermodynamic model involving argon and air species (O_2, N_2, O, N, NO) [11], we determine the composition and the temperature $T^*(Z)$ of the centerline plasma gas. Considering Prandlt and Schmit numbers close to 1, the Crocco integral throughout the mixing region of a plasma jet into quiescent air [12] then gives the centerline plasma velocity $U^*(Z) = \phi_{\rm Ar}(Z)\, U_o$ where the local argon volume fraction $\phi_{\rm Ar}(Z)$ is derived from mass spectrometry analysis. From gas sampling and mass spectrometry experiments, gas temperatures and velocities were determined on the centerline for net torch powers ranging from 300 W to 1800 W (Fig. 5). About two diameters downstream of the nozzle exit ($Z > 2D$), the ambient cold fluid penetrates into the jet centerline and the turbulent mixing results in a jet spreading proportional to Z/D. Both the centerline nondimensional temperature $T^*(Z)/T_O$ and velocity $U^*(Z)/U_O$ then roughly scale as D/Z (Fig. 5) in agreement with experiments from Huang *et al.* [13] and predictions from a two-fluid model for a turbulent plasma jet [14].

3 Particle levitation in argon plasma jet

The equilibrium levitation height Z increases with the net torch power P and the gas flow rate $\mathcal{Q}$ but also depends on the circular nozzle dimension and the sphere diameter d (Fig. 6). A decrease of the nozzle diameter D results in a thinner jet and an increase of the equilibrium levitation height since the particle intercepts a higher gas momentum flux. The experimental accuracy for the equilibrium levitation height is about 5%. Under low torch power conditions or for large nozzle diameters, the levitation is quite unstable since the particle takes a low position in the plasma jet. The lower equilibrium levitation height $Z \approx 2D$ then corresponds to the jet's inviscid core where plasma velocity is constant and shear gradients cancel.

On the basis of the work of Neve *et al.* [15], we define the plasma gas momentum flux J_O at the torch nozzle and we consider the dimensionless levitation height Z/D. The drag force F_D may be derived from the integration of the local gas momentum flux $\rho(r,\, Z,\, T)U^2(r,\, Z)$ over the frontal area of the particle exposed to the plasma flow:

$$\frac{F_D}{J_o} \approx \frac{4C_d \int_0^{d/2} 2\pi r \rho(r,\, z) U^2(r,\, z) dr}{\pi D^2 \rho_o U_o^2} \qquad (4)$$

with $J_o = \rho_o U_o^2 \pi D^2/4$ assuming very thin boundary layers in the nozzle and $C_d \approx 0.2$ for the drag coefficient around a stationnary sphere in a turbulent flow. In the downstream region of the jet, the turbulence intensity is

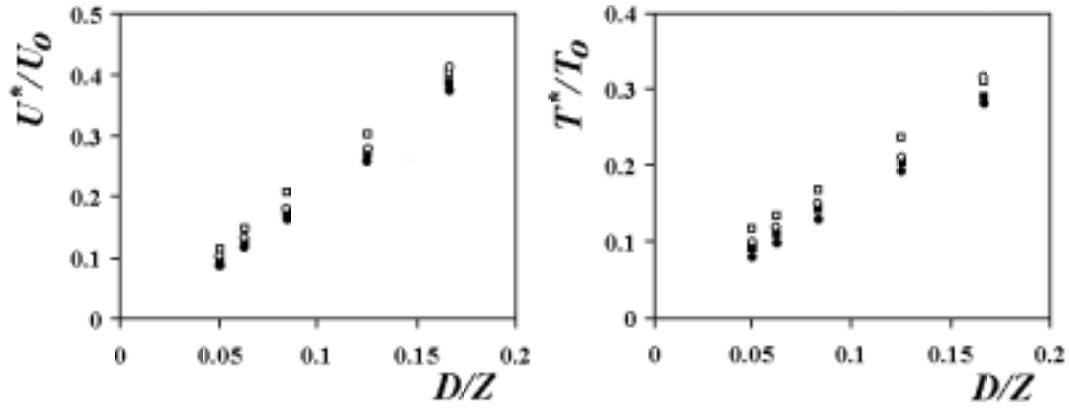

Fig. 5. Centerline dimensionless gas temperature $T^*(Z)/T_O$ and dimensionless gas velocity $U^*(Z)/U_O$ *versus* the dimensionless distance D/Z ($\mathcal{Q} = 8.4 \times 10^{-3}$ m^3/mn, $D = 3$ mm). (□) $P = 790$ W, (○) $P = 1050$ W, (■) $P = 1300$ W, (●) $P = 1780$ W.

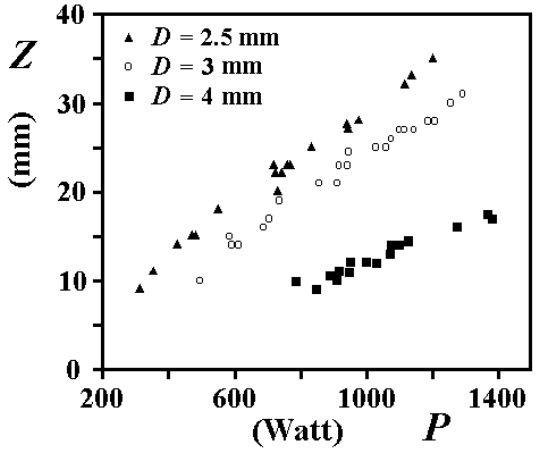

Fig. 6. Experimental variation of the equilibrium levitation height Z for a stainless steel spherical particle in argon plasma jet *versus* the net torch power P ($\mathcal{Q} = 7.56$ l/mn, $d = 7$ mm). (▲) $D = 2.5$ mm, (○) $D = 3$ mm, (■) $D = 4$ mm).

very high as reported by Goldschmidt and Eskinasi [16]. Under these conditions, the boundary layer around the particle is turbulent for Reynolds number above the subcritical value $2 \times 10^3 - 4 \times 10^3$ and then the drag coefficient approaches a constant value of 0.2 [17]. The Reynolds number $2 \times 10^3 < Re = U(Z)d\rho/\eta < 10^4$ for the flow around the sphere lies generally in the supercritical region (gas velocity 100 ms^{-1} $< U <$ 300 ms^{-1}, gas density 0.15 kg m^{-3} $< \rho <$ 0.25 kg m^{-3} and gas dynamic viscosity 4×10^{-5} kg m^{-1}s^{-1} $< \eta < 7.5 \times 10^{-5}$ kg m^{-1}s^{-1}), above the subcritical value. However, the Reynolds number may be slightly lowered when considering a turbulent viscosity higher than the molecular viscosity.

We further neglect the Mach number dependence of both the critical Reynolds number and the drag coefficient since the Mach number around the particle never exceeds the critical value $M = 1$ [18].

Considering the dimensional expression of gas temperature $T(r, z) \approx T^*(Z/D)\psi(r/D)$ in the plasma jet ($T^*(Z/D)$ is the gas temperature along the jet axis), the gas density $\rho(r, Z, T)$ then becomes:

$$T(r, z) \approx T^*(Z/D)\psi(r/D) \approx T_o \frac{D}{Z}\psi(r/D)$$
$$\rho(r, Z, T) \approx \rho_o \frac{T_o}{T^*\left(\frac{Z}{D}\right)\Psi\left(\frac{r}{D}\right)} \approx \rho_o \frac{Z}{D\Psi\left(\frac{r}{D}\right)}. \quad (5)$$

Equations (4) and (5) together with the dimensional expression of the gas velocity $U(r, Z) \approx U^*(D/Z)\ \Psi(r/D) \approx U_o\Psi(r/D)D/Z$ then yields the dimensionnless drag force F_D/J_0 acting on the rotating particle:

$$\frac{F_D}{J_o} = \frac{mg}{J_o} \approx 4C_d\frac{D}{Z}\int_0^{d/2D} x\Psi(x)dx \quad \text{for} \quad Z > 2D. \quad (6)$$

In agreement with equation (6), the experimental data indeed show a linear variation of the function mg/J_0 with the reduced downstream distance D/Z (Fig. 7a):

$$\frac{F_D}{J_o} = \frac{mg}{J_o} \approx \alpha\left(\frac{d}{D}\right)\frac{D}{Z} \approx 0.328\left(\frac{d}{D}\right)^{0.8}\frac{D}{Z} \quad (7)$$

where the plasma velocity U_0 and the gas momentum J_0 near the jet exit are determined from equation (5). The efficiency factor α only depends on the dimensionless parameter d/D and scales as $(d/D)^{0.8}$ (Tab. 1 and Fig. 7b). Such a dependence gives a local gas velocity $U(r, Z) = U^*(Z)\Psi(r/D)$ scaling as $(r/D)^{-1.2}$ for $r > 0$ and $Z > 2D$.

4 Heat transfer around a particle in argon plasma jet

The convective heat transfer coefficient h between a spherical particle of uniform temperature T_p and a plasma jet obeys the thermal balance:

$$hS\left(T - T_p\right) = mC_p\left(dT_p/dt\right) + \sigma\varepsilon_p S\left(T_p^4 - T_a^4\right) \quad (8)$$

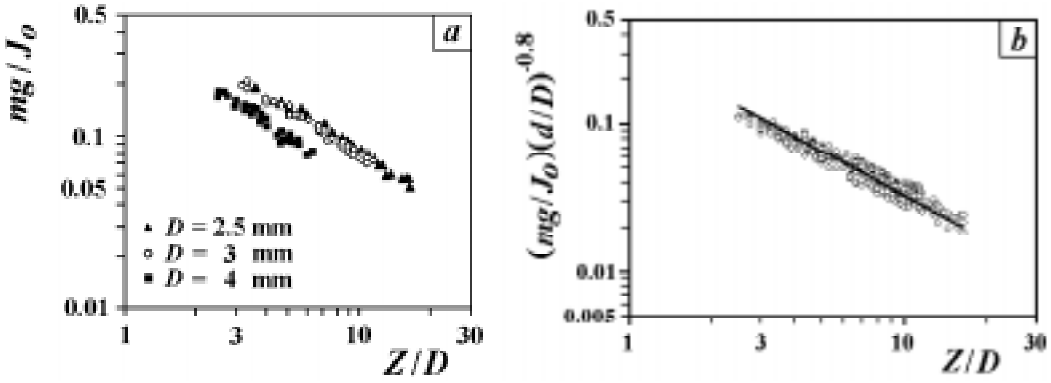

Fig. 7. Experimental variation of mg/J_o (a) and $(mg/J_o)(d/D)^{-0.8}$ (b) with the reduced downstream distance Z/D for various operating conditions ($d = 7$ mm, 2.5 mm $< D <$ 4 mm, 5×10^{-3} m^3/mn $< \mathcal{Q} < 1.1 \times 10^{-2}$ m^3/mn, 250 W $< P <$ 1500 W).

Table 1. Experimental values of the efficiency factor $\alpha(d, D)$.

d (mm)	6.5		7			7.5			8		
D (mm)	2.5	3	2.5	3	4	2.5	3	4	2.5	3	4
α	0.61	0.45	0.64	0.52	0.47	0.79	0.66	0.51	0.78	0.59	0.55

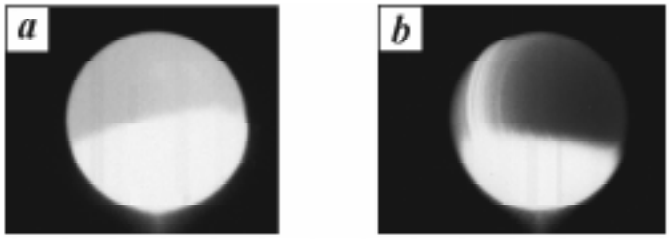

Fig. 8. Views of a particle levitated in argon plasma jet for a net torch power $P = 1000$ W (view (a) with $Z/D \approx 8$) or $P = 400$ W (view (b) with $Z/D \approx 3$). ($d = 7$ mm, $D = 3$ mm). Note that plasma reflections on the particle artificially increase the luminosity of the bottom region of the sphere.

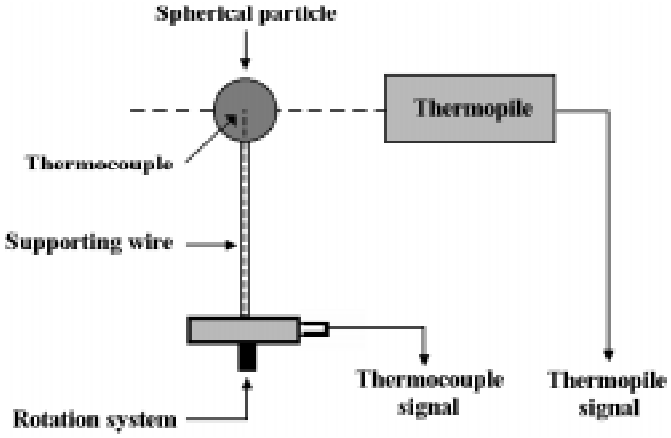

Fig. 9. Schematic drawing of the experimental setup for the temperature calibration of the thermopile.

where S is the particle area, C_p the steel heat capacity, σ the Stefan Boltzmann constant, ε_p the material emissivity, T a reference plasma temperature and T_a the ambient temperature. Steel particles were previously oxidized (blackened) in the plasma jet to eliminate any variation of the material total emissivity $\varepsilon_p \approx 0.85$ during the levitation experiments. The weak value of the Biot number $B = hd/(6\lambda_p) = Nu\lambda/(6\lambda_p) < 0.05$ (where $\lambda \approx 0.1$ W m^{-1} K^{-1} and $\lambda_p \approx 17.6$ W m^{-1} K^{-1} are respectively the thermal conductivity of argon plasma and particle material and $Nu < 50$ is derived from equation (1) with $Re < 9000$ and $Pr \approx 0.67$) and the rapid particle rotation in the plasma jet further implies that the equilibrium temperature distribution in the sphere is quite uniform [8,19]. The radiation light flux from the particle indeed appears as uniform over the sphere area ($P = 1$ kW, Fig. 8a). However, the surface temperature is less uniform under weak net torch power conditions. Under these conditions, only a ring shaped area is heated ($P = 0.4$ kW, Fig. 8b) since the particle is close to the nozzle and the jet has small lateral extent. We may further neglect the radiative heating of the particle by the optically thin plasma.

The surface temperature T_p of the particle was measured with ± 10 °C accuracy with an automatic optical pyrometer sensitive above 1100 °C (wavelength 650 nm) or with a thermopile in the low temperature regime.

The optical pyrometer analyses the light flux emitted by the rear surface of the particle through a return prism which makes negligible the plasma radiation and further renders the measurement less sensitive to spatial fluctuations of the steel sphere.

The thermopile consists of a reference surface and a blackened circular surface subject to the emission flux from the sphere. The temperature difference between surfaces scales as the radiation flux emitted by the particle. The temperature calibration was performed by imposing a rotation of an oxidized particle immersed in the plasma jet (Fig. 9) and measuring both the signals from the thermopile and the uniform sphere temperature with a thermocouple (type K) inserted into the rotating particle. The

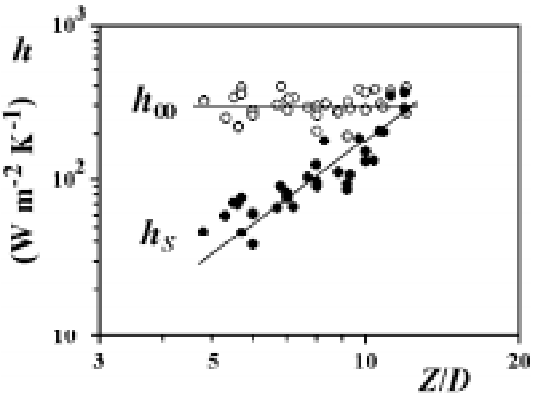

Fig. 10. Convective heat transfer coefficient *versus* the dimensionless levitation height Z/D. (•) h_S from experiments in stationary regime with a reference temperature $T^*(Z)$ at the front stagnation point. (○) h_∞ from experiments in transient regime.

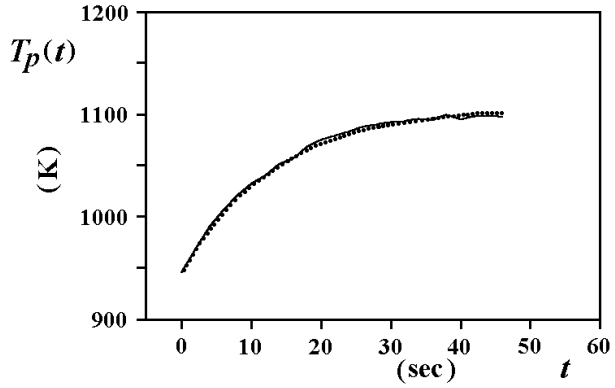

Fig. 11. Transient temperature signal $T_p(t)$ for a particle abruptly immersed in an argon plasma jet ($d = 7.5$ mm, $D = 2.5$ mm and $P = 600$ W). Experimental curve (−) and model curve derived from equation (8) with $h_\infty = 290$ W m^{-1}K^{-1} and $T_\infty = 1350$ K ($\cdots$).

steel particle was previously oxidized into the plasma jet to eliminate any variation of the surface emissivity during the levitation experiments. The emission E of the plasma surrounding the particle may be estimated from the analysis of the transient signal and remains lower than the particle emission E_p ($E/E_p < 15\%$) which ensures a ±5% accuracy for the temperature measurement above 900 K ($\delta T/T_p \approx \delta E/4E_p$).

In the stationary regime, the apparent convective heat transfer coefficient $h_S(Z)$ at the front stagnation point is determined from the surface temperature T_p and the centerline plasma temperature $T^*(Z)$ (reference plasma temperature):

$$h_S(Z) = \sigma\varepsilon_p \left(T_p^4 - T_a^4\right) / \left(T^*(Z) - T_p\right). \qquad (9)$$

As shown by visualization imagery of the plasma radiative flux with high gray level resolution [20] (Fig. 1a), the particle weakly perturbs the large scale plasma flow below the front stagnation point, and the gas temperature $T^*(Z)$ may be considered as a reference local temperature. The apparent convective heat transfer coefficient h_S increases with the levitation height and scales as $(Z/D)^{1.7}$ (Fig. 10).

The convective heat transfer coefficient was further determined from the time variation analysis of the surface temperature $T_p(t)$ when the particle is abruptly immersed in the plasma jet (Fig. 11). Assuming no dependence of the convective heat transfer coefficient with the particle temperature, equation (8) is solved by a two dimensional simplex method giving the parameters (h_∞, T_∞) of the equivalent infinite flow for the best fit of the transient temperature data $T_p(t)$. The convective transfer coefficient $h_\infty \approx 280$ W m^{-2} K^{-1} (±45 W m^{-2} K^{-1} accuracy) deduced from transient experiments displays no significant dependence with the levitation height Z (Fig. 10). The Nusselt number $Nu_\infty = h_\infty d/\lambda(Z)$ further ranges from 20 to 50 (with thermal conductivity of the plasma gas 0.1 W m^{-1} K^{-1} $> \lambda(Z) >$ 0.04 W m^{-1} K^{-1} for $5 < Z/D < 15$) in rather good agreement with the predictions of the Ranz Marshall correlation for an infinite flow [4] ($25 < Nu = 2 + 0.6Re^{1/2}Pr^{1/3} < 52$ for $2 \times 10^3 < Re < 9 \times 10^3$ and Pr ≈ 0.67).

The constancy of the convective heat transfer coefficient in a nonuniform flow of finite extent is surprising and likely results from the sphere rotation in the plasma which forces the neighboring fluid to rotate within a closed streamline pattern about the particle. The streamline pattern near the solid sphere and the transfer coefficients are then insensitive both to the large scale flows and the particle axial position in the plasma jet.

On the other hand, the unperturbed plasma temperature $T^*(Z)$ and the apparent convective transfer coefficient h_S referred to the front stagnation point ignore the microscale plasma/particle interaction and poorly describe heat transfer phenomena. Indeed, the temperature T_∞ of the equivalent infinite flow is much less than the unperturbed plasma temperature $T^*(Z)$ at the front stagnation point (Fig. 11) since the rotating particle absorbs heat from the hot side of the temperature gradient and discharges it while passing through the cold side [8]. One can expect enhanced energy transport (high equivalent particle conductivity) and uniform surface temperature for a rotation Peclet number $Pe = d^2\omega/\alpha_p \gg 1$ where $\alpha_p = \lambda_p/(\rho_p C_p)$ is the particle thermal diffusivity. The rotation Peclet number for the levitation of a steel particle of 7 mm diameter in argon plasma jet is about 10^4 (with $\rho_p = 7900$ kg/m^3, $\lambda_p \approx 17.6$ W m^{-1} K^{-1}, $C_p \approx 5 \times 10^2$ J kg^{-1} K^{-1} and $\omega \approx 10^3$ s^{-1}). Under such experimental conditions, we may ignore the temperature gradient and consider an infinite flow to describe heat transfer from a rotating particle in a nonuniform plasma flow independently of the material conductivity. The gas temperature T_∞ of the equivalent infinite flow representative of the boundary layer temperature conditions is close to the unperturbed plasma temperature $T^*(Z + D)$ near the rear stagnation point (Fig. 12).

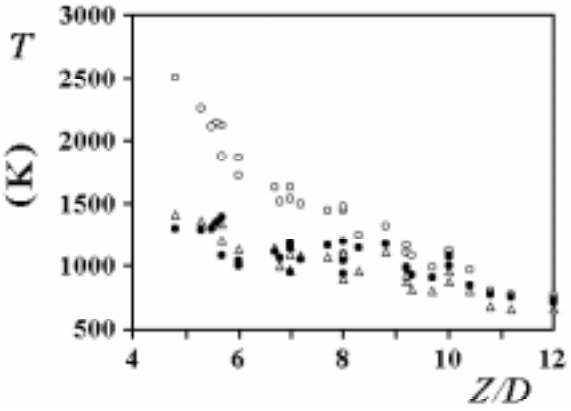

Fig. 12. Centerline plasma temperature *versus* the dimensionless downstream distance Z/D along the jet axis. (○) Undisturbed plasma temperature $T^*(Z)$ at the front stagnation point. (△) Undisturbed plasma temperature $T^*(Z+D)$ at the rear stagnation point, (•) Temperature T_∞ of the equivalent infinite flow derived from experiments in transient regime.

5 Conclusion

We have proposed a physical model for the aerodynamic levitation of a particle in a thermal plasma jet of finite extent. The heat transfer coefficient determined from the analysis of the transient temperature signal describes small scale particle/plasma interaction and shows no significant influence of the levitation height and the operative conditions because of the particle rotation and the uniform surface temperature. Therefore, we may consider an equivalent infinite flow to describe heat transfer between a rapidly rotating particle and a nonuniform plasma flow.

References

1. E. Pfender, Plasma Chem. Plasma Proc. **9**, 1675 (1989).
2. E.V. Seymour, Trans. ASME E: J. Appl. Mech., 739 (1971).
3. X. Chen, J.Y. Qiu, J. Yang, Plasma Chem. Plasma Proc. **11**, 151 (1991).
4. W.E. Ranz, W.R. Marshall, Chemical Eng. Prog. **48**, 173 (1952).
5. R.M. Young, E. Pfender, Plasma Chem. Plasma Proc. **7**, 2 (1987).
6. X. Chen, Pure Appl. Chem. **60**, 651 (1988).
7. G. Le Palec, M. Daguenet, Int. J. Heat Mass Transfer, **30**, 1511 (1987).
8. D.G. Wang, S.S. Satwinder, C.S. Campbell, Int. J. Heat Mass Transfer, **32**, 1413 (1989).
9. A. Ambari, B. Gautier-Manuel, E. Guyon, J. Fluid Mech. **149**, 235 (1984).
10. M. Announ, Ph.D. thesis, University of Perpignan France, 1996.
11. G. Eriksson, Acta Chem. Scand. **25**, 2651 (1971).
12. C.D. Donaldson, K.E. Gray, A.I.A.A. J. **4**, 2017 (1966).
13. P.C. Huang, W.L.T. Chen, J. Heberlein, E. Pfender, ISPC-10 Bochum **1**, 1 (1991).
14. P.C. Huang, J. Heberlein, E. Pfender, Plasma Chem. plasma Proc. **15**, 25 (1995).
15. R.S. Neve, R. Nelson, P. Kotsiopoulos, J. Fluid Mech. **107**, 521 (1981).
16. V. Goldsmith, S. Eskinazi, Trans. A.S.M.E. E: J. Appl. Mech. **33**, 735 (1966).
17. A.E. Achenbach, J. Fluid Mech. **54**, 565 (1966).
18. A. Naumann, Allgem. Warmetechnic, **4**, 217 (1953).
19. E. Bourdin, P. Fauchais, M. Boulos, Int. J. Heat Mass Transfer **26**, 257 (1983).
20. P. Snabre, A. Arahaliass, Appl. Optics **37**, 4017 (1998).